Check for updates

Phosphorescent cyclometalated platinum(II) complexes with phenyldiazine N^C ligands†

Mariia Hruzd,[a] Samia Kahlal,[a] Nicolas le Poul, [ID] [b] Laurianne Wojcik,[b] Marie Cordier,[a] Jean-Yves Saillard,[a] Julián Rodríguez-López, [ID] [c] Françoise Robin-le Guen,[a] Sébastien Gauthier [ID] *[a] and Sylvain Achelle [ID] *[a]

A series of phosphorescent platinum(II) complexes containing various phenyldiazine-type bidentate N^C ligands have been successfully synthesized and characterized. Structural modifications have been made to bidentate cyclometalating ligands regarding the nature of the diazine ring (pyrimidine, pyrazine and quinazoline), the substituent groups at the C4 position of the pyrimidine ring (OCH_3, CF_3) and the EDGs at the *para* position of the Pt atom (OCH_3, Ph, NPh_2, carbazol). In addition, the electronic properties of the azaheterocyclic ancillary ligand have been modulated in this series of complexes (pyridine, 4-methoxy-pyridine or pyrimidine). X-ray diffraction studies have been performed on three complexes, revealing Pt(II) ions in a distorted square-planar geometrical environment with no Pt(II)···Pt(II) interactions but with moderate π–π interactions in the solid-state structure. Electrochemical and computational studies suggest a ligand-centered reduction on the diazine ligands with, in some cases, additional contribution from the azaheterocyclic ancillary ligand, whereas oxidation occurs on the Pt-phenyl ring substituent moieties. All complexes exhibit phosphorescence emission ranging from green to red/near-infrared, both in solution and in the solid state. Complexes bearing a 2-(3-methoxyphenyl)pyrimidine ligand show the best PLQY of the series, up to 52% in a CH_2Cl_2 solution and 20% in the solid state. Furthermore, the solid state PLQY of one of the near-infrared emitting phenylquinazoline complex has been found to be 6%.

Introduction

Organic light emitting diodes (OLEDs), initially developed by Tang and VanSlyke,[1] have been a subject of intensive research over the last two decades because of their attractive application in flexible displays.[2] Due to the spin statistics, excitons are produced with a triplet : singlet ratio of 3 : 1, thus limiting the internal quantum efficiency (IQE) of fluorescent OLEDs to 25%.[3] A second generation of OLEDs, discovered in 1998,[4] based on phosphorescent emitters (PhOLEDs) has been extensively developed.[5] These materials can harvest both singlet and triplet excitons through direct trapping or an energy transfer process (intersystem crossing), leading to a theoretical IQE of 100%.[6] In this context, transition metal-based materials have been widely studied as phosphorescent emitters for OLEDs due to the strong spin–orbit coupling exhibited by the metal. Cyclometalated iridium(II) complexes are the benchmark emitters for PhOLEDs[7] but cyclometalated Pt(II) complexes have also been developed for this application.[8] The distinctive square-planar geometry of the Pt(II) complexes allows for intimate Pt(II)···Pt(II) contacts and intermolecular π–π stacking interactions, enabling metal–metal-to-ligand charge transfer (MMLCT) and excimer π–π* excited states.[9] This can have detrimental effects on photoluminescence properties, but can also be used for red or near-infrared emission.[10] Cyclometalated Pt(II) complexes have also been described for their thermally activated delayed fluorescence (TADF).[11]

The main classes of phosphorescent Pt(II) complexes are based on tridentate N^C^N or N^N^C ligands, with halogen and pseudo-halogen or acetylide ancillary ligands.[12] Platinum complexes with the bidentate N^C ligand are less in number and are often based on 2-phenylpyridine (ppy)-type ligands. They generally contain bidentate coligands such as acetylacetonate (acac).[13] Platinum(II) complexes bearing ppy-type N^C ligands with pyridine and chloride ancillary monodentate ligands have been frequently used as precursors for other

[a]Univ. Rennes, CNRS, ISCR (Institut des Sciences Chimiques de Rennes), UMR 6226, F-35000 Rennes, France. E-mail: sebastien.gauthier@univ-rennes1.fr, sylvain.achelle@univ-rennes1.Fr

[b]Université de Bretagne Occidentale, Laboratoire de Chimie, Electrochimie Moléculaires et Chimie Analytique, UMR CNRS 6521, UFR Science et Techniques, 6 Avenue Victor le Gorgeu, CS 93837 Brest Cedex 3, France

[c]Universidad de Castilla-La Mancha, Área de Química Orgánica, Facultad de Ciencias y Tecnologías Químicas, Avda. Camilo José Cela 10, 13071 Ciudad Real, Spain

luminescent ppy complexes.[14a,b] Recently, Zhao *et al.* have studied the photophysical properties of such complexes.[14c] The free rotation of the coordinated pyridine ligand reduced the efficiency of intersystem crossing and the radiative decay of the first triplet excited state (T_1) in solution, leading to low emission in solution. Nevertheless, the phosphorescence ability of these complexes was restored in a solid matrix, where the rotation of the pyridine ring could be restricted. Aggregation-induced phosphorescence has been demonstrated in these complexes and analogues bearing an acetylide ligand instead of chloride.[15] The non-planar conformation of the pyridine ring may prevent excimer formation in the solid state.

On the other hand, diazines are six-membered aromatic heterocycles with two nitrogen atoms. Depending on the position of N atoms, pyridazine (1,2-diazine), pyrimidine (1,3-diazine) and pyrazine (1,4-diazine) can be distinguished. The quinazoline ring corresponds to benzo-annulated pyrimidine. The diazine rings exhibit a stronger π-deficient character than pyridine due to the presence of a second N atom and have been used as the attracting part in numerous push–pull structures.[16]

For bidentate N^C ligands, the combination of the strong σ-donor effect of phenylate and the π-accepting character of the

azaheterocyclic ring has been shown to result in a high ligand-field for the coordinated metal, which increases the energy of quenching d–d states while reducing emissive metal-to-ligand charge transfer (MLCT) and ligand-centered excited states.[6a] In this context, the replacement of pyridine with diazine rings appears as an interesting option. Thus, it has been shown that a 2-(4-*N*,*N*-diphenylaminophenyl)pyrimidine Pt(II) complex bearing pyridine and chloride auxiliary ligands exhibits strong green phosphorescence emission in a solid matrix and promising electroluminescent properties.[14c] We have recently demonstrated that functionalization of 2-phenylpyrimidine with electron-donating groups (EDGs) at the *meta* position of the phenyl ring induces a bathochromic shift in the emission of the corresponding Pt(II) complexes associated with a significant increase in the intensity of phosphorescence in solution.[17]

In this contribution, we have designed a series of 24 Pt(II) complexes based on N^C phenyldiazine ligands and monodentate ancillary ligands (Chart 1). Various structural modifications have been made concerning the nature of the diazine ring (pyrimidine, pyrazine and quinazoline), the substituent groups at the C4 position of the pyrimidine ring, the EDGs at the *para* position of the Pt atom in the phenyldiazine ligand, and the azaheterocyclic ancillary ligand.
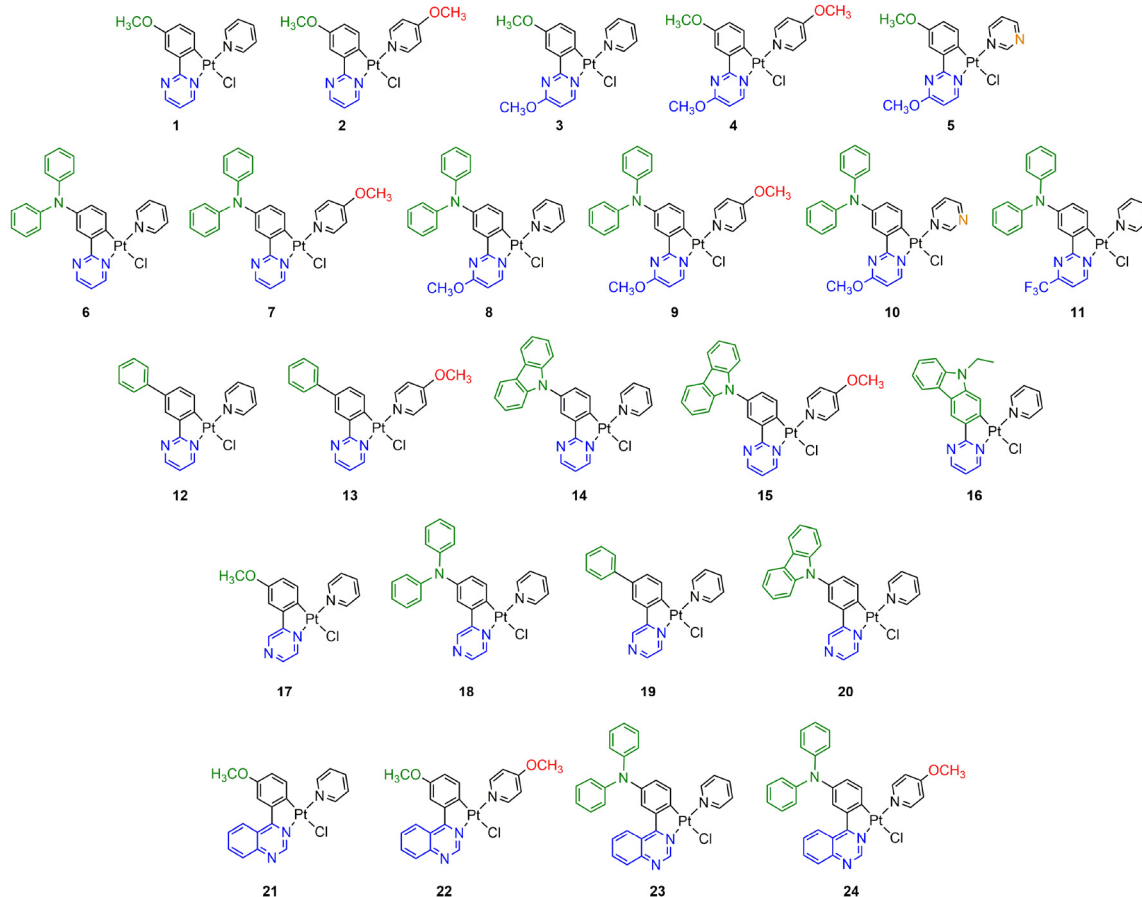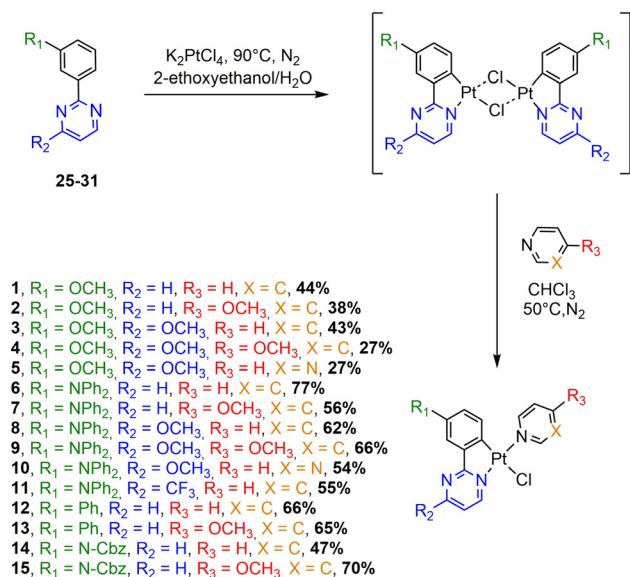

Chart 1 Chemical structures of the cyclometalated platinum-based complexes **1–24** investigated in this work.
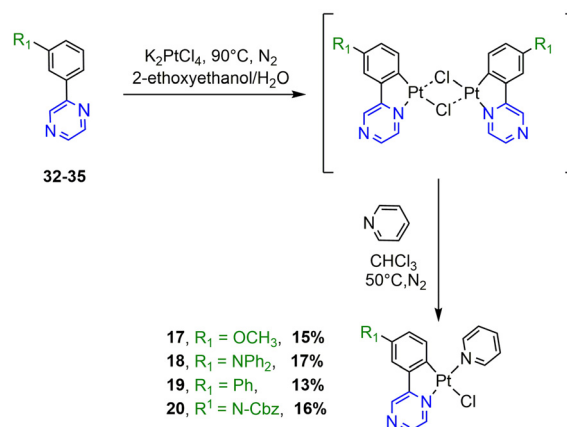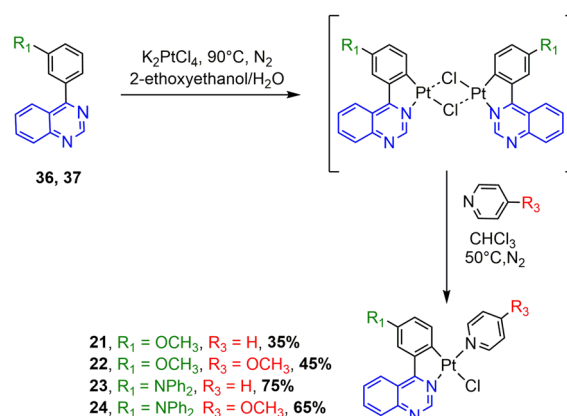
Results and discussion

Synthesis and characterization

The synthesis of the N^C ligands **25–38** was easily accomplished in good yields from commercially available chlorodiazine and the appropriate arylboronate ester derivatives. The Suzuki–Miyaura cross-coupling reaction was used according to a method previously reported in the literature (ESI, Scheme S1†).[16–18] The N^C cyclometalated chloro-Pt(II) complexes **1–24** were prepared according to the well-established method of synthesis for the traditional counterparts, by treating the Pt(II) μ-chloro-bridged dimer complexes with the pyridine, 4-methoxy-pyridine or pyrimidine ancillary ligand, in low to moderate yields (Schemes 1–4).[14] These air-stable compounds were isolated in high purity as solids after column chromatography on silica gel with the appropriate eluent. It should be noted that the yields of the complexes with phenyl-pyrazine ligands are significantly lower than those of their pyrimidine and quinazoline analogues due to the electronic effect of the second N atom in the conjugated position to the Pt atom. The N^C ligands **25–38** and chloro-platinum complexes **1–24** were characterized by NMR (^{1}H and ^{13}C) and high-resolution mass spectrometry (HRMS). The characterization data

1, R_1 = OCH$_3$, R_2 = H, R_3 = H, X = C, **44%**
2, R_1 = OCH$_3$, R_2 = H, R_3 = OCH$_3$, X = C, **38%**
3, R_1 = OCH$_3$, R_2 = OCH$_3$, R_3 = H, X = C, **43%**
4, R_1 = OCH$_3$, R_2 = OCH$_3$, R_3 = OCH$_3$, X = C, **27%**
5, R_1 = OCH$_3$, R_2 = OCH$_3$, R_3 = H, X = N, **27%**
6, R_1 = NPh$_2$, R_2 = H, R_3 = H, X = C, **77%**
7, R_1 = NPh$_2$, R_2 = H, R_3 = OCH$_3$, X = C, **56%**
8, R_1 = NPh$_2$, R_2 = OCH$_3$, R_3 = H, X = C, **62%**
9, R_1 = NPh$_2$, R_2 = OCH$_3$, R_3 = OCH$_3$, X = C, **66%**
10, R_1 = NPh$_2$, R_2 = OCH$_3$, R_3 = H, X = N, **54%**
11, R_1 = NPh$_2$, R_2 = CF$_3$, R_3 = H, X = C, **55%**
12, R_1 = Ph, R_2 = H, R_3 = H, X = C, **66%**
13, R_1 = Ph, R_2 = H, R_3 = OCH$_3$, X = C, **65%**
14, R_1 = N-Cbz, R_2 = H, R_3 = H, X = C, **47%**
15, R_1 = N-Cbz, R_2 = H, R_3 = OCH$_3$, X = C, **70%**

Scheme 1 Synthesis of N^C cyclometalated chloro-Pt(II) complexes **1–15**.

Scheme 2 Synthesis of N^C cyclometalated chloro-Pt(II) complex **16**.

17, R_1 = OCH$_3$, **15%**
18, R_1 = NPh$_2$, **17%**
19, R_1 = Ph, **13%**
20, R^1 = N-Cbz, **16%**

Scheme 3 Synthesis of N^C cyclometalated chloro-Pt(II) complexes **17–20**.

21, R_1 = OCH$_3$, R_3 = H, **35%**
22, R_1 = OCH$_3$, R_3 = OCH$_3$, **45%**
23, R_1 = NPh$_2$, R_3 = H, **75%**
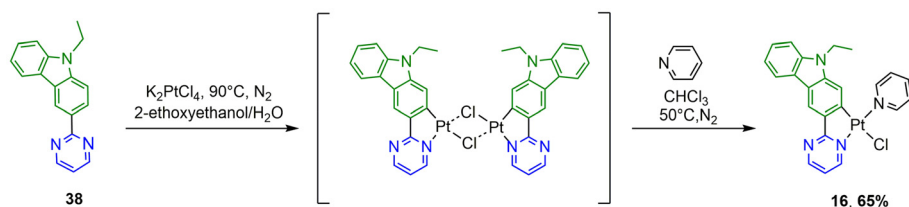24, R_1 = NPh$_2$, R_3 = OCH$_3$, **65%**

Scheme 4 Synthesis of N^C cyclometalated chloro-Pt(II) complexes **21–24**.

were found to be in complete agreement with the proposed structures as detailed in the ESI.†

X-ray crystal structures

Single crystals of chloro-platinum complexes **7**, **12**, and **14** were obtained by slow evaporation of a hexane/ethyl acetate (2/1) solution of the complex at room temperature. Their molecular structures were determined by X-ray crystallography analysis (Fig. 1 and S63, S64†). The crystal data and
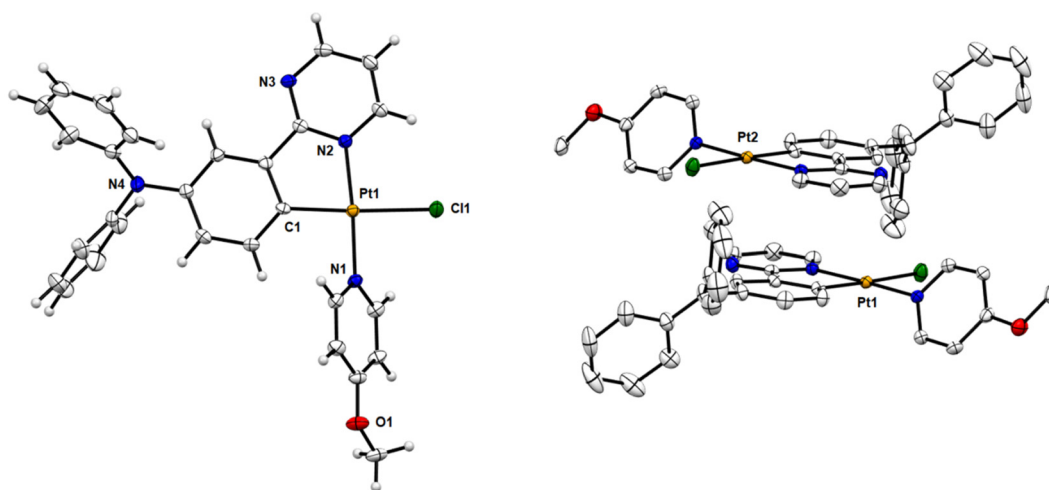
Fig. 1 ORTEP representation of complex **7** (left) with 50% ellipsoid probability. All co-crystallized solvent molecules have been omitted for clarity. ORTEP representation of the crystal packing structure in the dimeric form: complex **7** (right) showing head-to-tail configuration. Thermal ellipsoids are set at the 50% probability level. Hydrogen atoms and all co-crystallized solvent molecules have been omitted for clarity.

Table 1 Selected X-ray bond distances (Å) and angles (°) of complexes **7**, **12**, and **14**. Corresponding DFT-computed values are given in brackets

	7	**12**	**14**
Pt1–C1	1.988(3) [1.983]	1.990(3) [1.982]	1.988(3) [1.982]
Pt1–N1	2.025(3) [2.027]	2.021(3) [2.025]	2.010(3) [2.025]
Pt1–N2	2.028(3) [2.018]	2.017(3) [2.019]	2.017(3) [2.020]
Pt1–Cl1	2.3890(9) [2.421]	2.3952(9) [2.418]	2.3874(9) [2.416]
C1–Pt1–N1	94.66(12) [95.6]	95.33(13) [95.6]	95.38(13) [95.5]
C1–Pt1–N2	81.23(12) [81.1]	81.51(3) [81.1]	81.19(13) [81.1]
N1–Pt1–N2	175.86(10) [176.6]	176.84(11) [176.7]	176.29(12) [176.6]
C1–Pt1–Cl1	176.56(10) [176.3]	175.57(10) [176.3]	177.26(11) [176.4]
N1–Pt1–Cl1	88.70(10) [88.1]	88.62(9) [87.9]	87.17(9) [88.1]
N2–Pt1–Cl1	95.41(8) [95.3]	94.54(9) [95.3]	96.24(9) [95.3]
Pt⋯Pt	5.144	5.815	10.051
π–π	~3.40	~3.51	—^{a}

^{a} No significant π–π interactions.

structure refinement details are provided in the ESI (Tables S1–S3†), and selected bond lengths and angles are listed in Table 1. As can be seen from the X-ray structures, the central platinum ion is coordinated to a bidentate cyclometalating N^C ligand and two monodentate ligands (chloride and pyridine). The coordination sphere of the Pt(II) cation in all complexes (**7**, **12**, and **14**) adopts a distorted square-planar geometry with *trans*-C,Cl, *trans*-N,N chelating disposition, characteristic of d^8 metal complexes. The C1–Pt1–N2 angles (81.19–81.51°) are found to deviate from the ideal angle 90° due to the restricted bite angle of the bidentate C^N ligands. This is accompanied by a concomitant opening of the C1–Pt1–N1 (94.66–95.38°) and N1–Pt1–Cl1 (87.17–88.70°) bond angles. The bonds chelating around the platinum ion exhibit typical bond lengths compared with some similar complexes.[14,15,19]

Fig. 1 and S64† show that complexes **7** and **12** are packed as head-to-tail dimers in crystals. The closest Pt–Pt distances ($d_{Pt–Pt}$) in the crystals of **7** and **12** are 5.144 Å and 5.815 Å respectively, indicating the absence of metal–metal interactions. However, the dimers have slight overlap between the adjacent [Pt(C^N)] moieties with a vertical plane-to-plane separation ($d_{π–π}$) of ~3.40 Å for **7** and ~3.51 Å for **12**, indicative of moderate π–π interactions for these two complexes. Notably, the molecules of complex **14** are packed as head-to-tail dimers in the crystal packing with one co-crystallized ethyl acetate solvent molecule between two Pt complexes. No significant Pt(II)⋯Pt(II) or π–π interactions could be detected, since the closest Pt–Pt distance is 10.051 Å with no direct overlap between adjacent complexes.

Electrochemical properties

Voltammetric studies were carried out in CH_2Cl_2 in order to decipher the redox properties of the complexes in relation with their photophysical features. Table 2 gathers the electrochemical data using a Pt working electrode. All complexes show several oxidation peaks above 0.3 V *vs.* Fc$^+$/Fc and one reduction peak below *ca.* −1.6 V (see Fig. 2 and ESI Fig. S65–S70† for cyclic voltammograms).

As a first observation, it seems clear that the nature of the diazine ring significantly affects the reduction potential of the complexes. This is best exemplified by the methoxy series (complexes **1**, **17**, **21**), which shows reduction peaks at −2.27 V (pyrimidine), −1.97 V (pyrazine), and −1.67 V (quinazoline) against Fc$^+$/Fc, respectively. The potential difference of 300 mV between each of these complexes (Fig. 2A) can be correlated with the electronic properties of diazine, with the most electron deficient system (quinazoline) moving the reduction peak towards the most positive values. Compared to the pyrimidine derivative, the annulated benzene ring of the quinazoline

Table 2 Electrochemical data for complexes **1–24** (C = 0.5 mM) using a Pt working electrode in 0.1 M NBu$_4$PF$_6$ in CH$_2$Cl$_2$ (E/V *vs.* Fc, ν = 0.1 V s^{-1})

Complex	$E°(1)$	$E_{pa}(2)$	$E°(3)$
1		0.78[a]	−2.27[a]
2		0.75[a]	−2.29[a]
3		0.75[a]	−2.39[a]
4		0.70[a]	−2.40[a]
5		0.83[a]	−2.26[a]
6	0.36	0.58[b]	−2.25[a]
7	0.35	0.62[b]	−2.21[a]
8	0.35	0.56[b]	−2.36[a]
9	0.33	0.63[b]	−2.40[a]
10	0.39	0.57[b]	−2.24[a]
11	0.42	1.12[a]	−1.84
12		1.01[a]	−2.21[a]
13		0.92[a]	−2.27[a]
14		0.85[a]	−2.28[a]
15		0.75[a]	−2.24[a]
16		0.50	−2.27[a]
17		0.82[a]	−1.97
18	0.40	1.05[a]	−1.97[a,c]
19		1.02[a]	−1.96[a]
20		0.82[a]	−1.94[a]
21		0.82[a]	−1.67
22		0.77[a]	−1.69
23	0.42	1.04[a]	−1.67
24	0.40	1.00[a]	−1.68

[a] Irreversible peak (E_{pa} or E_{pc} value). [b] Low-intensity wave which becomes more intense after reduction at −2.3 V. [c] A supplementary low-intensity reversible wave is detected at −1.42 V upon reduction.

system probably favors electron delocalization upon electrochemical reduction, leading to better stabilization of the reduced species.[13c] Another interesting observation is that both pyrazine and quinazoline complexes exhibit a reversible reduction process, whereas the pyrimidine complex exhibits a completely irreversible reduction process. Such irreversibility may be caused by the reaction between the reduced complex and the electrolytic solution. The process could also be interpreted as a disproportionation reaction involving the reduced pyrimidine complex.[20]

Voltammetric studies were also carried out with complexes bearing various substituents at the 4-position of the pyrimidine ring. A striking result was obtained with the trifluoromethyl substituted complex **11**. Indeed, the reduction process occurs at a much less negative potential compared to the H-substituted pyrimidine complex **6** (410 mV difference) (Fig. 2B).

On the oxidation side, the presence of a diphenylamino group on the Pt-bound phenyl moiety (complexes **6–11**) induces the appearance of a reversible wave at *ca.* $E°(1)$ = 0.35 V, which can be ascribed to the oxidation of the amine.[14c] The different substituents at the *para* position of the phenyl ring in relation to the Pt metal center affect the oxidation potential according to their electron donating properties. Therefore, the lowest oxidation potential value was obtained for the strongest electron-donating NPh$_2$ group: phenyl (**12**: 1.07 V); 9*H*-carbazol-9-yl (**14**: 0.90 V); methoxy (**1**: 0.78 V), and diphenylamino (**6**: 0.58 V).

The redox properties of the present complexes can be compared with those already reported by Zhao and co-workers[14c] for an analogous 2-phenylpyrimidine complex with the diphenylamino group at the *meta* position of the Pt atom. Although the voltammetric behavior is similar, the first two oxidation peaks for complex **6** are found at much less positive values (approx. 300 mV). This discrepancy may be ascribed to the difference in the position of the diphenylamino group on the phenyl ring, which may affect both the amine and Pt(II) oxidation processes. In the cathodic part of the voltammogram, both complexes show irreversible reduction peaks at around −2.2 V (170 mV difference). Accordingly, this process was proposed to occur primarily at the pyrimidine and ancillary pyridine groups. Further comparison can be made with tridentate C^N^N–Pt complexes. For example, complexes **1** and **5** display oxidation peaks at more positive potential values than the reported N^C^N–Pt chloro analogue, where N = pyrimidine and C = methoxybenzene.[12f] Conversely, the reduction occurs at more negative values. Even if the comparison is not strictly
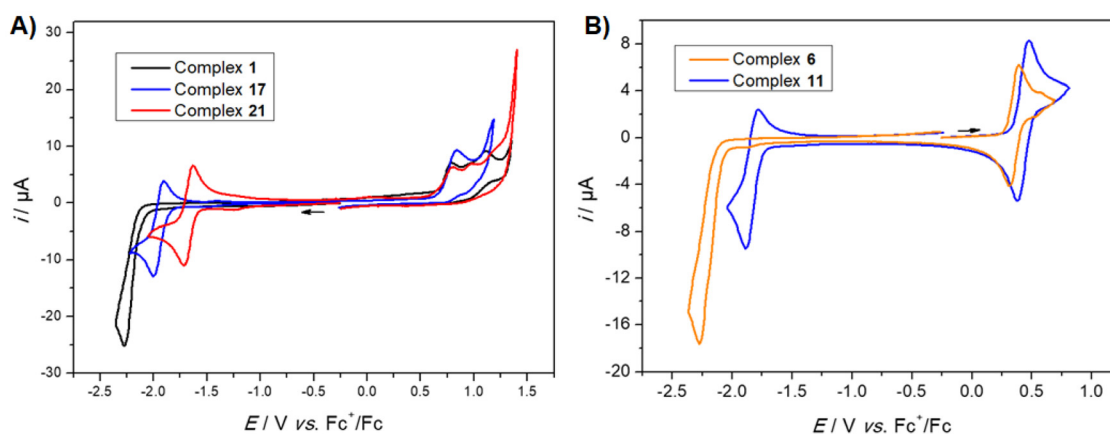

Fig. 2 (A) Cyclic voltammograms of complexes **1** (black), **17** (blue), and **21** (red). (B) Cyclic voltammograms of complexes **6** (orange) and **11** (blue). CV obtained by using a Pt working electrode in 0.1 M NBu$_4$PF$_6$ in CH$_2$Cl$_2$ (E/V *vs.* Fc$^+$/Fc, ν = 0.1 V s^{-1}, C = 0.5 mM). The arrow indicates the scanning direction from the initial potential.

Open Access Article. Published on 12 January 2023. Downloaded on 1/24/2026 6:41:05 PM. This article is licensed under a Creative Commons Attribution-NonCommercial 3.0 Unported Licence.

Paper

correct, this difference suggests that the tridentate structure stabilizes the oxidized and reduced states and lowers the HOMO–LUMO gap compared to the bidentate case.

Photophysical properties

The UV/vis absorption and photoluminescence properties of complexes were measured in degassed CH_2Cl_2 solution and in potassium bromide pellets (2 wt%). The resulting data are summarized in Table 3.

Several absorption bands at below 400 nm are observed for all complexes, with the most intense one being attributed to intraligand $n–\pi^*$ and $\pi–\pi^*$ transitions.[17] Furthermore, one or, in some cases, two significantly less intense bands appear between 400 and 570 nm. The absorption spectra of phenylpyrimidine complexes 1, 6, 12, and 14 are shown in Fig. 3 (see the ESI, Fig. S71–S76† for other complexes). These bands have metal-to-ligand charge transfer (MLCT) and ligand-to-ligand charge transfer (LLCT) character. In the phenylpyrimidine series, the less energetic absorption band red-shifts with increasing the strength of the electron-donating group at the *para* position of the Pt atom on the phenyl moiety: from 404 nm for phenyl (12) to 412 nm for 9H-carbazol-9-yl (14), 427 nm for methoxy (1), and 449 nm for diphenylamino (6). The same trend is observed in the phenylpyrazine and phenyl-quinazoline series. 9H-carbazol-2-yl-pyrimidine complex 16

exhibits a less energetic absorption band that is red-shifted compared to those of all the phenylpyrimidine analogues. In the phenylpyrimidine series, the presence of an electron-donating methoxy group on the pyrimidine ring induces a slight blue-shift of up to 18 nm (1, 2, 6, and 7 *vs.* 3, 4, 8, and 9 respectively). On the other hand, a strong electron-withdrawing trifluoromethyl group on the pyrimidine ring (compound 11) induces a red-shift of 28 nm regarding 6 (Fig. S72†). Meanwhile, in the pyrimidine series, a change in the ancillary ligand (pyridine with 4-methoxypyridine or pyrimidine) does not significantly modify the position of the absorption band.

Phenylpyrazine and phenylquinazoline analogues have a less energetic absorption band that is notably red-shifted as can be seen, for example, in the methoxy series: 427 nm for the phenylpyrimidine complex 1, 466 nm for the phenylpyrazine complex 17, and 504 nm for the phenylquinazoline complex 21 (Fig. S73†). It has been reported that this bathochromic shift can be explained by the presence of a second N atom in the conjugated position to the Pt atom in the pyrazine complexes,[22] and by the more pronounced electron-withdrawing character of the quinazoline fragment.[18a]

Most of the complexes are luminescent in CH_2Cl_2 solutions with emission lifetimes ranging from 4 to 12 µs and Stokes shifts between 4700 and 6300 cm^{-1}, characteristic of phosphorescence. The presence of strong electron-donating diphe-

Table 3 Photophysical characteristics of complexes 1–24 in CH_2Cl_2 and in the solid state (2 wt% in the KBr matrix)

	CH_2Cl_2 [a]					KBr (2 wt%)		
	UV/Vis	PL				PL		
	λ_{max}, nm (ε, mM^{-1} cm^{-1})	λ_{max}, nm	τ, µs	Φ_{PL}[b], %	Stokes shift[c], cm^{-1}	λ_{max}, nm	τ, µs	Φ_{PL}[d], %
1	254 (42.3), 294 (14.0), 347 (6.22), 427 (2.95)	556, 582	12.9	45	5434	531, 593	14.8	4
2	254 (40.9), 289 (13.9), 351 (5.55), 430 (2.55)	556, 582	9.7	54	5553	551, 589	11.6	20
3	253 (46.0), 297 (10.8), 341 (5.89), 416 (4.57)	545, 575	12.0	47	5404	547, 577	13.2	3
4	252 (38.5), 288 (18.4), 338 (5.04), 415 (2.99)	545, 575	7.7	15	5632	562, 594	9.6	2
5	251 (28.8), 285 (14.3), 345 (4.69), 413 (2.49)	543, 571	4.3	9	5797	587	9.6	<1
6	258 (24.4), 293 (35.2), 449 (2.92)	643	8.9	5	6744	635	9.7	2
7	258 (25.0), 294 (35.0), 451 (3.13)	643	7.4	4	6474	630	15.6	8
8	259 (30.6), 293 (38.5), (5.71), 437 (1.67)	630	6.8	8	6523	625	13.6	5
9	262 (33.6), 293 (50.0), 350 (8.24), 433 (2.17)	630	6.1	6	6422	604	10.9	3
10	259 (19.9), 292 (28.7), 342 (6.53), 442 (1.74)	630	6.0	3	6498	598, 627	13.4	5
11	255 (24.1), 299 (44.4), 345 (3.57), 383 (1.45) 477 (0.84)	642	—[e]	<1	—[e]	691	9.9	2
12	277 (41.3), 346 (3.94), 404 (1.27)	508, 538	8.5	5	4705	495, 531, 566	12.0	7
13	277 (35.1), 348 (4.06), 402 (1.79)	508, 538	4.4	7	6253	517$_{sh}$, 555, 590	11.5	3
14	241 (68.9), 261 (52.5), 291 (38.7), 341 (10.6), 412 (2.29)	547	4.7	12	5990	517, 568	12.2	5
15	270 (36.4), 330 (9.11), 342 (10.0), 415 (2.46)	543	3.9	15	6094	567	13.2	14
16	271 (26.7), 298 (12.0), 341 (14.1), 379 (8.33), 455 (1.84)	583	7.3	22	5040	630	14.5	1
17	256 (33.0), 319 (13.1), 357 (7.82), 466 (2.12)	630	6.3	12	5725	634, 699	17.4	4
18	264 (53.5), 283 (60.0), 372 (4.31), 490 (1.57)	—[e]	—[e]	—[e]	—[e]	684	7.4	2
19	270 (61.2), 321 (19.6), 347 (11.9), 445 (2.55)	583	7.9	30	6275	652	14.6	3
20	243 (56.8), 267 (53.6), 328 (13.2), 343 (10.6), 452 (1.02)	608	5.6	9	5928	638	10.5	2
21	274 (29.4), 351 (10.5), 401 (4.53), 504 (3.32)	671	5.4	26	4975	728	9.2	3
22	246 (21.3), 259 (23.1), 276 (22.4), 351 (8.05), 367 (7.53), 408 (3.98), 511 (3.13)	677	5.1	16	4776	720	6.3	6
23	280 (48.9), 299 (49.8), 345 (24.8), 364 (16.0), 397 (6.71), 546 (2.79), 563 (3.17)	—[e]	—[e]	—[e]	—[e]	795	3.5	<1
24	247 (24.6), 292 (38.9), 364 (12.9), 396 (6.44), 566 (3.23)	—[e]	—[e]	—[e]	—[e]	—[e]	—[e]	—[e]

[a] All spectra were recorded at room temperature at $c \sim 1.0 \times 10^{-5}$ M. The solutions were deoxygenated by bubbling N_2. [b] Photoluminescence quantum yield (±10%) determined in relation to 9,10-bisphenylethynylanthracene in cyclohexane ($\Phi_{PL} = 1.00$).[21] [c] Calculated using the less energetic absorption and the more energetic emission bands. [d] Absolute value measured with an integrating sphere (powder). [e] Emission too low to permit accurate measurement.
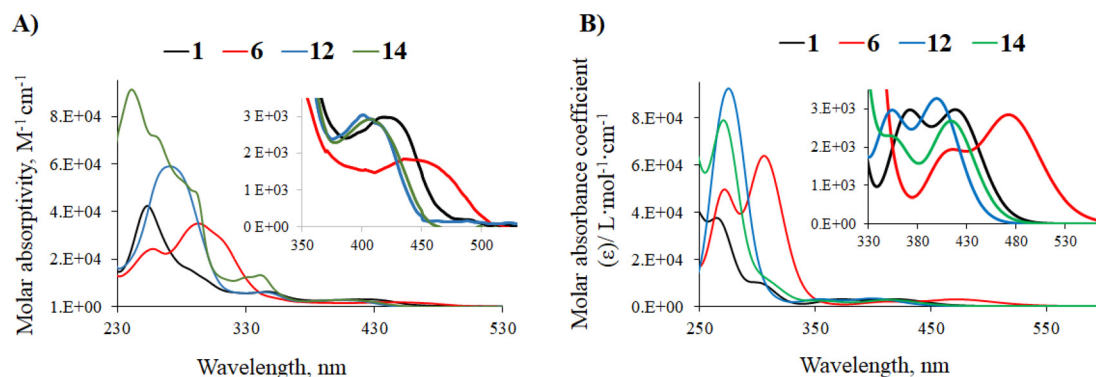
Fig. 3 (A) UV-Vis absorption spectra of phenylpyrimidine complexes **1**, **6**, **12**, and **14** in CH_2Cl_2 solution ($C \sim 10^{-5}$ M). (B) TD-DFT-simulated UV-vis absorption spectra of complexes **1**, **6**, **12**, and **14**.

nylamino groups on the phenylpyrazine/phenylquinazoline ligands (complexes **18**, **23**, and **24**) leads to non-emissive complexes. The latter may be explained by a too strong charge transfer that disfavors the radiative return to the ground state.[23] The position of the emission band in the phenylpyrimidine complexes follows the same trend as that in the less energetic absorption band; a red-shift is observed as the strength of the electron-donating substituent increases: green emission for phenyl (**12**, 508/538 nm), yellow-green for 9*H*-carbazol-9-yl (**14**, 547 nm), yellow for methoxy (**1**, 556/582 nm), and red for diphenylamino group (**6**, 644 nm) (Fig. 4). In this series, the highest PLQY is observed for the methoxy complex **1** (45%). Complex **16** with the 9*H*-carbazol-2-yl-pyrimidine N^C ligand shows yellow-orange emission with a PLQY of 22%. The presence of a methoxy substituent on the pyrimidine ring induces a slight blue-shift (8–17 nm) of the emission (complexes **1**, **2**, **6**, and **7** *vs.* **3**, **4**, **8**, and **9**, respectively) due to the reduction of the electron-withdrawing character of the heterocyclic part of the N^C ligand. In the phenylpyrimidine series,
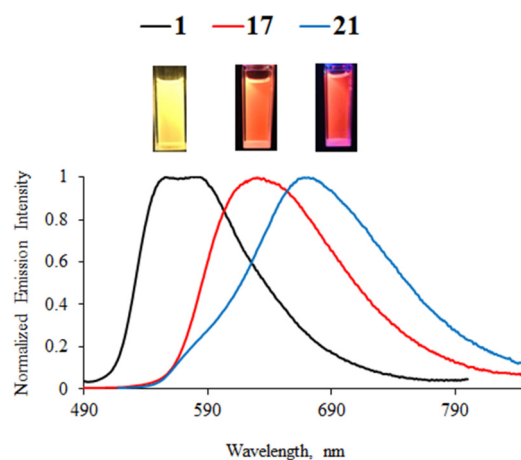

Fig. 5 Normalized emission spectra of methoxy-substituted complexes **1**, **17**, and **21** in deoxygenated CH_2Cl_2 solution ($C \sim 10^{-5}$ M). $\lambda_{exc} = \lambda_{max}^{abs}$ of the lowest energy band. Inset: Picture of the CH_2Cl_2 solutions taken under UV irradiation (from left to right: **1**, **17**, and **21**).
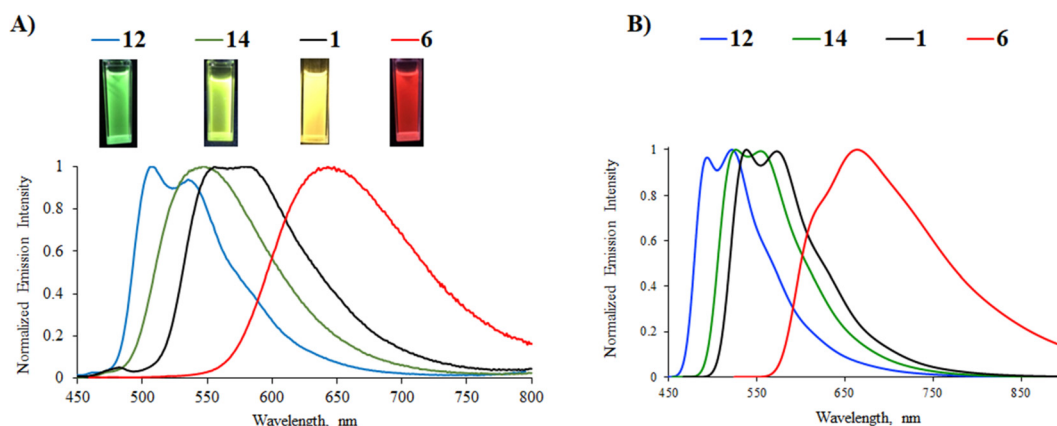

Fig. 4 (A) Normalized emission spectra of phenylpyrimidine complexes **1**, **6**, **12**, and **14** in deoxygenated CH_2Cl_2 solution ($C \sim 10^{-5}$ M). $\lambda_{exc} = \lambda_{max}^{abs}$ of the lowest energy band. Inset: Pictures of the CH_2Cl_2 solutions taken under UV irradiation (from left to right: **12**, **14**, **1**, and **6**). (B) DFT-simulated phosphorescence spectra of complexes **12**, **14**, **1**, and **6**.
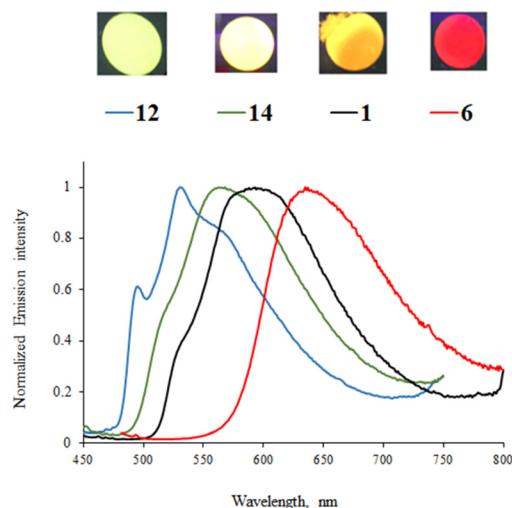
Fig. 6 Solid state emission (2 wt% in the KBr matrix) of complexes **1**, **6**, **12**, and **14**. $\lambda_{exc} = \lambda_{max}^{abs}$ of the lowest energy band in CH_2Cl_2 solution. Inset: Pictures of the KBr pellets taken under UV irradiation (from left to right: **12**, **14**, **1**, and **6**).

the modification of the azaheterocyclic ancillary ligand does not appreciably change the emission maxima (**2**, **4/5**, **7**, and **9/10** vs. **1**, **3**, **6**, and **8**, respectively), although the pyrimidine ligands (complexes **5** and **10**) significantly decrease the PLQY.

Phenylpyrazine complexes **17**, **19**, and **20** exhibit a red-shift of around 60 nm in relation to their phenylpyrimidine analogues and exhibit lower PLQY. As for the methoxy-substituted complex **17**, the emission is shifted to the orange-red region of the spectrum (Fig. 5). The emission of the methoxy-substituted

phenylquinazoline complex **22** is the most red-shifted in the series ($\lambda_{em} = 678$ nm).

Emission can also be detected for all complexes in the solid state (2 wt% in the KBr matrix), except for **24**. Emission lifetimes are higher than those in CH_2Cl_2 solution (up to 17.4 µs for **17**). As an example, the emission spectra of complexes **1**, **6**, **13**, and **14** are shown in Fig. 6. As in solution, the solid-state emission depends on the substituents on the phenyl ring and the nature of the diazine ring. No particular red-shift or broadening of the emission band is observed, which could indicate aggregation or excimer formation, probably because the out-of-plane azaheterocyclic ancillary ligand hinders Pt(II)···Pt(II) and π–π interactions. Nevertheless, the emission from the pyrazine and quinazoline complexes **17–22** is red-shifted for up to 80 nm in relation to the emission in solution.

The position of emission maxima globally follows the same rules as that in CH_2Cl_2 solution. The highest PLQYs are measured for complexes **2** (20%), **15** (14%), and **7** (8%), all of them bearing the 4-methoxypyrimidine ancillary ligand. Phenylquinazoline complexes **21–23** exhibit emission in the near-infrared region and the PLQY of complex **22** (6%) is particularly appealing for such emission.

Computational investigations

Density functional theory (DFT) calculations at the PBE0/Def2-TZVP level were performed to optimize the geometries of compounds **1–24**, except for complex **16**. Solvent (CH_2Cl_2) effect corrections were included (see the Computational details in the ESI†). The optimized structures are shown in Fig. S91 and S92.† The optimized geometries of **6**, **12**, and **14** are in a very good agreement with their experimental X-ray results (see

Table 4 Relevant computed data for complexes **1–15** and **17–23**. The reported λ_{max} values are taken from the simulated spectra

Complex	μ (D)	ΔE_{H-L} (eV)	IE[a] (eV)	EA[b] (eV)	λ_{max} (nm) absorption	λ_{max} (nm) emission
1	5.94	3.86	5.54	−2.30	265, 372, 418	538
2	6.90	3.87	5.51	−2.27	304, 275, 418	540
3	7.04	3.95	5.50	−2.24	249, 306, 406	533
4	7.45	3.95	5.47	−2.21	263, 312, 408	571
5	7.99	3.86	5.56	−2.29	246, 309, 408	567
6	4.07	3.36	5.10	−2.35	306, 417, 472	664
7	5.82	3.38	5.08	−2.33	305, 409, 472	651
8	5.18	3.47	5.09	−2.29	269, 306, 459	692
9	6.56	3.48	5.07	−2.27	307, 356, 457	607
10	6.44	3.36	5.13	−2.35	309, 353, 465	678
11	6.99	3.05	5.16	−2.74	376, 461, 526	682
12	4.11	4.02	5.75	−2.33	275, 355, 400	522
13	5.29	4.02	5.72	−2.30	279, 353, 402	496
14	3.58	3.76	5.56	−2.41	240, 270, 413	526
15	5.48	3.79	5.55	−2.39	308, 355, 412	550
17	9.04	3.60	5.57	−2.59	249, 294, 465	590
18	8.85	3.21	5.16	−2.56	305, 370, 503	713
19	7.26	3.76	6.20	−2.62	283, 441	538
20	6.33	3.50	5.60	−2.69	241, 279, 452	571
21	10.87	3.28	5.58	−2.92	274, 326, 513	672
22	10.95	3.28	5.55	−2.90	327, 357, 515	729
23	9.36	2.80	5.15	−2.95	353, 410, 595	805
24	10.22	2.82	5.14	−2.93	317, 412, 592	951

[a] Electron affinity. [b] Ionization energy.

Table 1 and compare Fig. 1 with Fig. S91 and S92†). Relevant computed data are provided in Table 4. The largest HOMO–LUMO gaps (ΔE_{H-L} = 4.02 eV) are found for complexes with phenyl-substituted pyrimidine ligands **12** and **13**, whereas the smallest HOMO–LUMO gap (3.05 eV) corresponds to **11**, which bears both donor (diphenylamino) and acceptor (trifluoromethyl) substituents. The HOMOs of all the complexes are similar (see selected examples in Fig. 7). They show little or no involvement of the pyridine and pyrimidine heterocycles. Assuming that the C–Pt–Cl axis is the x axis and z is perpendicular to the Pt coordination plane, they all consist of some $5d_{xz}$(Pt) atomic orbitals (AOs) (typically between 7 and 30%) antibondingly mixed with π-type orbitals of the ligands co-

ordinated along the x axis. This ligand contribution to the HOMOs is predominant. The HOMOs of the complexes that bear a diphenylamino substituent on the phenyl ring show a large participation of this substituent, which explains their peculiar oxidation behavior (see above). For all complexes, there is only one occupied orbital with dominant metal participation. It is $5d_{z^2}$ in nature and, depending on the complexes, corresponds to the HOMO−1, HOMO−2 or HOMO−3 (see the selected MO diagrams in Fig. S100–S104†). The formally occupied $5d_{xy}$, $5d_{xz}$ and $5d_{yz}$ AOs are in fact diluted in a large number of the occupied molecular orbitals (down to the HOMO−10/HOMO−14), in which the ligand character always dominates. The LUMOs of all the complexes are derived from
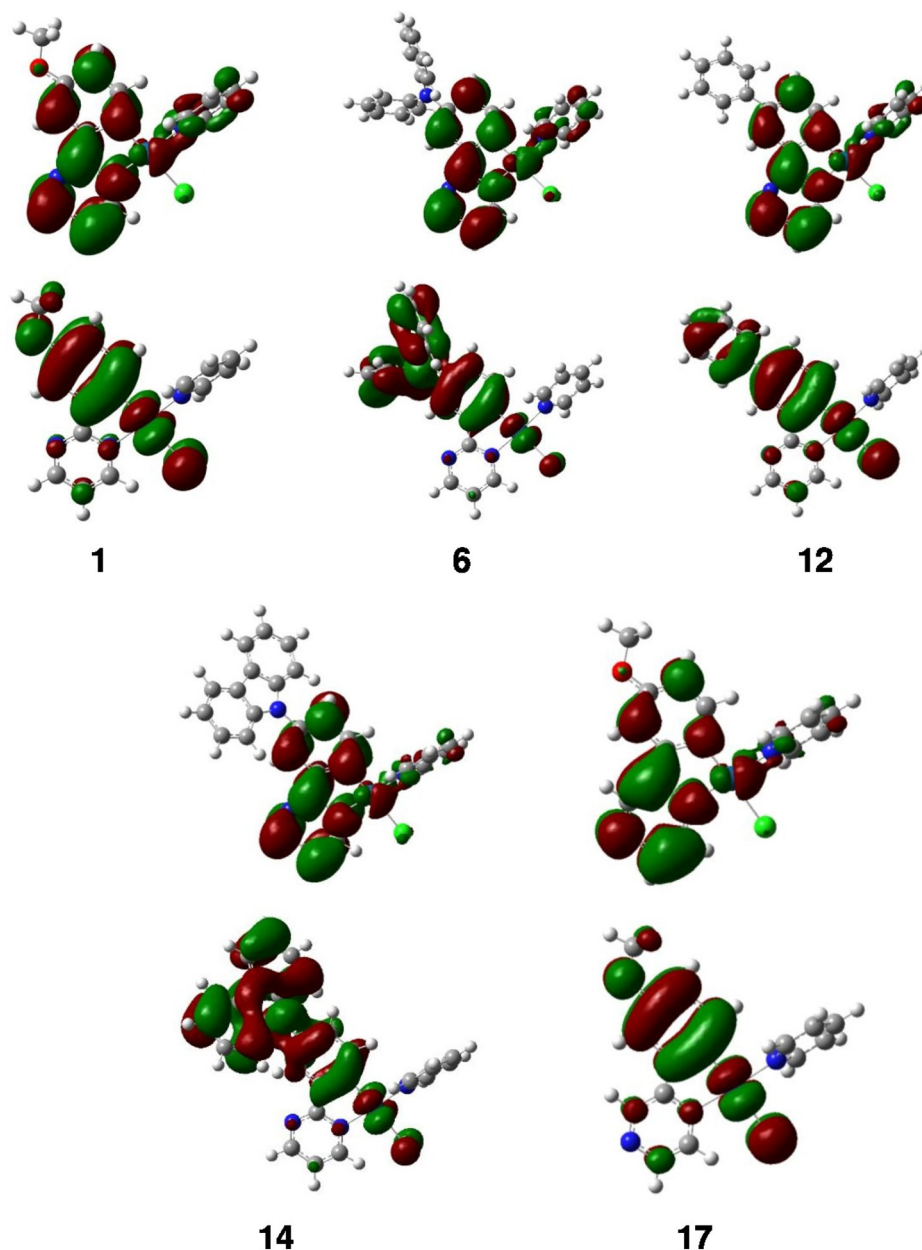

Fig. 7 Plots of the HOMO (below) and LUMO (above) of complexes **1**, **6**, **12**, **14**, and **17**.

the LUMOs of the diazine ligands, with a small percentage of metal participation, and, in some cases, additional contribution from the azaheterocyclic ancillary ligands (Fig. 7).

The computed ionization energies correlate linearly with the first recorded oxidation peak (see above), except for compounds **12**, **14**, and **19**, for which the match is more approximate (see Fig. S93†). In the case of these three compounds, a peculiarly explicit role of the electrolyte or solvent in the cationic form, not considered in the calculations, could be tentatively predicted. There is also a slightly lower correlation between the computed electron affinities and the recorded E° (3) potentials (Fig. S94†). It should be noted that most of the electrochemical potentials considered in Fig. S93 and S94† correspond to the irreversible peaks (see Table 2), which could be the reason for the appearance of some (small) deviations away from the root-mean-square line.

TD-DFT calculations were performed for complexes **1–24** (except for **16**) to better understand their optical behavior. The simulated spectra (singlet → singlet transitions) satisfactorily reproduce the shape of the experimental spectra and their λ_{max} values (Table 4) match reasonably well with their recorded counterparts (Table 3). The simulated spectra of **1**, **6**, **12**, and **14** are illustrated in Fig. 3 and those of the other complexes are shown in Fig. S95–S97.† For all of them, the weak band of the lowest energy with $\lambda_{max} > 400$ nm is associated with a HOMO–LUMO transition. The higher energy bands are majorly LLCT in nature (mainly with L = substituted diazine) with some MLCT contribution, owing to the (minor but significant) metallic admixture of most of the highest occupied molecular orbitals (MOs). It should be noted that the occupied MO, mostly of $5d_z^2$ in nature, is not involved in these transitions.

It was found that the fully optimized lowest triplet state simply results from a HOMO → LUMO excitation. The vibrationally resolved simulated phosphorescence spectra were computed by assuming emission from this excited state (see the Computational details). The simulated spectra of complexes **1**, **6**, **12**, and **14** match quite well with their experimental counterparts recorded in solution (Fig. 4). The λ_{max} values obtained from the simulated spectra are listed in Table 4 where a fairly good agreement can be observed between most of these values and the corresponding experimental ones (Table 3 and Fig. S105†). It can also be noted that the computed values for the experimentally non-emissive complexes **19**, **23**, and **24** fall in the near-infrared region. The value corresponding to **11** (also non-emissive) is slightly smaller (682 nm).

The charge transfers associated with the triplet → singlet emission were calculated from TD-DFT calculations by using the method developed by Adamo and coworkers[24] (see the Computational details). They are quantified by their corresponding transferred fractions of electron q^{CT} over associated spatial extends d^{CT}. They are illustrated as the plots of the differences between the densities of the two states involved in the emission process, which are shown along with their associated q^{CT} and d^{CT} in Fig. S98 and S99.† Their main features indicate a charge transfer from the substituted phenyl ring to the diazine heterocycle. The non-emissive compounds **11**, **18**, **23**, and **24** are

still different from the other complexes with their larger q^{CT} and d^{CT} values. It is noteworthy that the complexes having the largest PLQY in CH_2Cl_2 solution (namely **1**, **2**, and **3**) are among those with the lowest q^{CT} and d^{CT}, which is surprising at the first glance. Nevertheless, it should be considered that important charge reorganisations are also associated with non-negligible structural changes upon de-excitation, which in turn tend to favor non-radiative processes. Compounds **1–3** appear to satisfy the best balance between such conflicting parameters.

Conclusion

In summary, we have designed a series of 24 Pt(II) complexes bearing phenyldiazine N^C ligands as well as chloride and azaheterocyclic ancillary ligands. The remarkable feature of the here presented material is that a rather simple structural motif of the Pt(II) complex was successfully modified, yielding interesting luminophores. Various structural modifications have been made in this series of complexes: the substituent on the phenyl ring at the *para* position to the metal center (methoxy, diphenylamino, phenyl, and 9*H*-carbazol-9-yl), the nature of the diazine fragment (pyrimidine, pyrazine, and quinazoline), the substituents at the C4 position of the pyrimidine ring (OMe and CF_3), and the nature of the azaheterocyclic ancillary ligand (pyridine, 4-methoxypyridine and pyrimidine). The structural modifications have a significant effect on the optical properties of the complexes, which exhibit green to red/near-infrared phosphorescence emission both in CH_2Cl_2 solution and in the solid state. The following structure–property relationships can be highlighted:

• The strength of the EDG on the phenyl ring tunes the oxidation potential, the HOMO energy and emission wavelength. The stronger the EDG, the more red-shifted the emission.

• The nature of the diazine fragment affects the reduction potential and the emission wavelength, with a red-shift in the following order: pyrimidine < pyrazine < quinazoline. For pyrimidine complexes, both the reduction potential and the emission wavelength can be modulated by introducing an EDG/EWG at the C4 position of the pyrimidine ring.

• The ancillary ligand has a moderate influence on the electronic properties but plays a significant role in the PLQY. In the solid state, the 4-methoxypyridine ligand has a beneficial effect.

Complexes **1–3** with a 2-(3-methoxyphenyl)pyrimidine ligand exhibit the best compromise in terms of charge transfer, leading to the best PLQY (up to 52% in CH_2Cl_2 solution). On the other hand, phenylquinazoline complexes **21–23** exhibit emissions in the near-infrared region. The solid-state PLQY of complex **22** (6%) is particularly appealing for such red-shifted emissions. In the near future, more attractive complexes will be incorporated in PhOLED devices.

Conflicts of interest

There are no conflicts to declare.

Acknowledgements

References

1 C. W. Tang and S. A. VanSlyke, *Appl. Phys. Lett.*, 1987, **51**, 913.

2 (*a*) R.-P. Xu, Y.-Q. Li and J.-X. Tang, *J. Mater. Chem. C*, 2016, **4**, 9116; (*b*) A. Salehi, X. Fu, D.-H. Shin and F. So, *Adv. Funct. Mater.*, 2019, **29**, 1808803; (*c*) N. T. Kalyani and S. J. Dhoble, *Renewable Sustainable Energy Rev.*, 2012, **16**, 2696; (*d*) G. Hong, X. Gan, C. Leonhardt, Z. Zhang, J. Seibert, J. M. Busch and S. Bräse, *Adv. Mater.*, 2021, **33**, 2005630.

3 M. A. Baldo, D. F. O'Brien, M. E. Thompson and S. R. Forrest, *Phys. Rev. B: Condens. Matter Mater. Phys.*, 1999, **60**, 14422.

4 M. A. Baldo, D. F. O'Brien, Y. You, A. Shoustikov, S. Sibley, M. E. Thompson and S. R. Forrest, *Nature*, 1998, **395**, 151.

5 H. Sasabe and J. Kido, *Eur. J. Org. Chem.*, 2013, 7653.

6 (*a*) C. Adachi, M. A. Balto, M. E. Thompson and S. R. Forrest, *J. Appl. Phys.*, 2001, **90**, 5048; (*b*) P. T. Chou and Y. Chi, *Chem. – Eur. J.*, 2007, **13**, 380.

7 (*a*) Y. Yo and S. Y. Park, *Dalton Trans.*, 2009, 1267; (*b*) E. Baranoff, J.-H. Yum, M. Graetzel and Md. K. Nazeeruddin, *J. Organomet. Chem.*, 2009, **694**, 2661; (*c*) M. G. Helander, Z. B. Wang, J. Qiu, M. T. Greiner, D. P. Puzoo, Z. W. Liu and Z. H. Lu, *Science*, 2011, **332**, 944.

8 (*a*) J. Kalinnowski, V. Fattori, M. Cocchi and J. A. G. Williams, *Coord. Chem. Rev.*, 2011, **255**, 2401; (*b*) C. Cebrián and M. Mauro, *Beilstein J. Org. Chem.*, 2018, **14**, 1459.

9 (*a*) V. W.-W. Yam, K. M.-C. Wong and N. Zhu, *J. Am. Chem. Soc.*, 2002, **124**, 6506; (*b*) K. M.-C. Wong and V. W.-W. Yam, *Acc. Chem. Res.*, 2011, **44**, 424; (*c*) P. Pander, A. Sil, R. J. Salthouse, C. W. Harris, M. T. Walden, D. S. Yufit, J. A. G. Williams and F. B. Dias, *J. Mater. Chem. C*, 2022, **10**, 15084.

10 (*a*) M. Ibrahim-Ouali and F. Dumur, *Molecules*, 2019, **24**, 1412; (*b*) S. F. Wang, L.-W. Fu, Y.-C. Wei, S.-H. Liu, J.-A. Lin, G.-H. Lee, P.-T. Chou, J.-Z. Huang, C.-I. Huang, C.-I. Wu, Y. Yuang, C.-S. Lee and Y. Chi, *Inorg. Chem.*, 2019, **58**, 13892; (*c*) S. F. Wang, Y. Yuan, Y.-C. Wei, W.-H. Chan, L.-W. Fu, B.-K. Su, I.-Y. Chen, K.-J. Chou, P.-T. Chen, H.-F. Hsu, C.-L. Ko, W.-Y. Hung, C.-S. Lee, P.-T. Chou and Y. Chi, *Adv. Funct. Mater.*, 2020, **30**, 2002173.

11 (*a*) P. Pander, R. Daniels, A. V. Zaytsev, A. Horn, A. Sil, T. J. Penfold, J. A. G. Williams, V. N. Kozhevnikov and F. B. Dias, *Chem. Sci.*, 2021, **12**, 6172; (*b*) P. Pander, A. V. Zaytsev, A. Sil, J. A. G. Williams, V. N. Kozhevnikov and F. B. Dias, *J. Mater. Chem. C*, 2022, **10**, 4851; (*c*) P. Pander, A. V. Zaytsev, A. Sil, J. A. G. Williams, P.-H. Lanoe, V. N. Kozhevnikov and F. B. Dias, *J. Mater. Chem. C*, 2021, **9**, 10276.

12 (*a*) M. Hruzd, S. Gauthier, J. Boixel, S. Kahlal, N. le Poul, J.-Y. Saillard, S. Achelle and F. Robin-le Guen, *Dyes Pigm.*, 2021, **194**, 109622; (*b*) A. Haque, L. Xu, R. A. Al-Balushi, M. K. Al-Suti, R. Ilmi, Z. Guo, M. S. Khan, W.-Y. Wong and P. R. Raithby, *Chem. Soc. Rev.*, 2019, **48**, 5547; (*c*) P. K. Chow, G. Cheng, G. S. M. Tong, W.-P. To, W.-L. Kwong, K.-H. Low, C.-C. Kwok, C. Ma and C.-M. Che, *Angew. Chem., Int. Ed.*, 2015, **54**, 2084; (*d*) F. Nisic, A. Colombo, C. Dragonetti, D. Roberto, A. Valore, J. M. Malicka, M. Cocchi, G. R. Freeman and J. A. G. Williams, *J. Mater. Chem. C*, 2014, **2**, 1791; (*e*) Z. Wang, E. Turner, V. Mahoney, S. Madakuni, T. Groy and J. Li, *Inorg. Chem.*, 2010, **49**, 11276; (*f*) M. Hruzd, N. le Poul, M. Cordier, S. Kahlal, J.-Y. Saillard, S. Achelle, S. Gauthier and F. Robin-le Guen, *Dalton Trans.*, 2022, **51**, 5546.

13 (*a*) M. Z. Shafikov, R. Daniels, P. Pander, F. B. Dias, J. A. G. Williams and V. N. Kozhevnikov, *ACS Appl. Mater. Interfaces*, 2019, **11**, 8182; (*b*) G. Zhou, Q. Wang, X. Wang, C.-L. Ho, W.-Y. Wong, D. Ma, L. Wang and Z. Lin, *J. Mater. Chem.*, 2010, **20**, 7472; (*c*) J. Brooks, Y. Babayan, S. Lamansky, P. I. Djurovich, I. Tsyba, R. Bau and M. E. Thompson, *Inorg. Chem.*, 2002, **41**, 3055.

14 (*a*) Y. Sun, C. Zhu, S. Liu, W. Wang, X. Chen, G. Zhou, X. Yang and W.-Y. Wong, *Chem. Eng. J.*, 2022, **449**, 137457; (*b*) M. Chaaban, S. Lee, J. S. R. Vellore Winfred, X. Lin and B. Ma, *Small Struct.*, 2022, **3**, 2200043; (*c*) J. Zhao, F. Dang, Z. Feng, B. Liu, X. Yang, Y. Wu, G. Zhou, Z. Wu and W.-Y. Wong, *Chem. Commun.*, 2017, **53**, 7581.

15 (*a*) J. Zhao, Z. Feng, D. Zhong, X. Yang, Y. Wu, G. Zhou and Z. Wu, *Chem. Mater.*, 2018, **30**, 929; (*b*) X. Yang, L. Yue, Y. Yu, B. Liu, J. Dang, Y. Sun, G. Zhou, Z. Wu and W.-Y. Wong, *Adv. Opt. Mater.*, 2020, **8**, 2000079; (*c*) H. Yang, H. Li, L. Yue, X. Chen, D. Song, X. Yang, Y. Sun, G. Zhou and Z. Wu, *J. Mater. Chem. C*, 2021, **9**, 2334.

16 (*a*) S. Achelle, J. Rodríguez-López and F. Robin-le Guen, *ChemistrySelect*, 2018, **3**, 1852; (*b*) P. Meti, H.-H. Park and Y.-D. Gong, *J. Mater. Chem. C*, 2020, **8**, 352; (*c*) R. Plaza-Pedroche, D. Georgiou, M. Fakis, A. Fihey, C. Katan, F. Robin-le Guen, S. Achelle and J. Rodríguez-López, *Dyes Pigm.*, 2021, **185**, 108948.

17 M. Fecková, S. Kahlal, T. Roisnel, J.-Y. Saillard, J. Boixel, M. Hruzd, P. le Poul, S. Gauthier, F. Robin-le Guen, F. Bureš and S. Achelle, *Eur. J. Inorg. Chem.*, 2021, 1592.

18 (*a*) S. Achelle, J. Rodríguez-López and F. Robin-le Guen, *J. Org. Chem.*, 2014, **79**, 7564; (*b*) K. Hoffert, R. J. Durand, S. Gauthier, F. Robin-le Guen and S. Achelle, *Eur. J. Org. Chem.*, 2017, 523.

19 H. Fukuda, Y. Yamada, D. Hashizume, T. Takayama and M. Watabe, *Appl. Organomet. Chem.*, 2009, **23**, 154.

20 N. Elgrishi, K. J. Rountree, B. D. McCarthy, E. S. Rountree, T. T. Eisenhart and J. L. Dempsey, *J. Chem. Educ.*, 2018, **95**, 197.

21 M. Taniguchi and J. S. Lindsey, *Photochem. Photobiol.*, 2018, **94**, 290.

22 S. Culham, P.-H. Lanoë, V. L. Whittle, M. C. Durrant, J. A. G. Williams and V. N. Kozhevnikov, *Inorg. Chem.*, 2013, **52**, 10992.

23 Y. Chen, K. Li, W. Lu, S.-Y. Chui, C.-W. Ma and C.-M. Che, *Angew. Chem., Int. Ed.*, 2009, **48**, 9909.

24 (*a*) T. Le Bahers, C. Adamo and I. Ciofini, *J. Chem. Theory Comput.*, 2011, **7**, 2498; (*b*) I. Ciofini, T. Le Bahers, C. Adamo, F. Odobel and D. Jacquemin, *J. Phys. Chem. C*, 2012, **116**, 11946; (*c*) D. Jacquemin, T. Le Bahers, C. Adamo and I. Ciofini, *Phys. Chem. Chem. Phys.*, 2012, **14**, 5383.